Acoustic measurements of cavitation and inception in tip leakage flow

Patrick S. Russell[1], Luka Barbaca[1], James A. Venning, Bryce W.Pearce, and Paul A. Brandner

University of Tasmania, Launceston TAS 7250, AUS, patrick.russell@utas.edu.au

Abstract. High Reynolds number tip leakage flow is examined in a variable pressure water tunnel for a range of incidences, gap heights, cavitation numbers and free-stream cavitation nuclei populations. Acoustic measurements alongside high-speed imaging capture the prevalence of cavitation which is shown to be complex and often intermittent. It is a product of the combined effects of the strength of the leakage flow and hence vortex strength, the nature of the nuclei population, and the relative thickness of the wall boundary layer to the tip gap clearance. Persistence of cavitation in the leakage vortex is sustained by three main influences. The event rate of new cavities, the duration for which a cavity can be sustained, and the speed at which an established cavity is advected downstream. These processes affect the character of the measured acoustic emissions. These vary from persistent to intermittent bursts of noise for which temporal and spectral analyses are required depending on flow conditions.

Keywords: Tip-Leakage · Cavitation · Experimental · Inception · Hydrophone

1 Introduction

Tip leakage flows observed in pumps, ducted propulsors and turbomachinery are characterized by a strong primary vortex, composed of many merging co-rotating sub-vortices, and a plethora of weaker secondary vorticity [24].
Efforts to understand cavitation in tip-leakage flow have been renewed after recent investigations on the nature of inception in structured turbulent flows [2, 1, 6]. A liquid may locally come under tension due to the strong pressure drop at the core of a vortex [3]. Studies have shown that in the majority of conditions, pure water can sustain considerable tension before inception occurs [29]. However, should tension coincide with the presence of a suitable nucleus (such as a gas bubble) cavitation inception within the vortex may occur [21].
Such cavitation often forms in the vortices shed from a lifting surface or in the turbulent shear layer flows. The stochastic character of the shear layer flows renders the activation of a specific nuclei an unlikely event, as the trajectory of a nuclei and presence of a vortex core with suitable tension must be spatio-temporally coincident [2, 20]. This likelihood may increase when a vortex retains

a coherent structure, due to an increase in the opportunity for a bubble to be transported into the vortex core via buoyancy. Recent studies have shown that inception often occurs due to complex unsteady interactions within vortical system, where weaker vortices are rapidly stretched around stronger ones [6]. Vortex stretching produces necking along the axis of the core increasing circulation and reducing its radius, thus resulting in an instantaneous spike in low pressure. Tip leakage flows observed in pumps, ducted propulsors and turbomachinery readily provide such conditions. Their topology is characterized by strong primary vorticies, composed of many merging co-rotating sub-vortices, and a plethora of weaker secondary vorticity [24]. These structures interact, but also capture nuclei from a large cross-section of the flow [27], further increasing the probability of inception to occur. Cavitation inception in these flows is usually assessed using acoustic measurements. Incipient and developed vortical cavitation structures can exhibit complex dynamics as cavitation bubbles interact with the surrounding flow [10–12]. Bubble cavitation phenomena, such as growth, deformation, fragmentation, and collapse, can lead to narrow and/or broadband sound acoustic emissions [17, 18].

Cavitation inception can often be determined using simple spectral analysis of acoustic data. However, incipient structures may impart a very weak signature that is spread over a range frequencies, spectral analysis may become insensitive for conditions where both amplitude and the event rate are low. To improve the detection algorithm, more complex analysis tools for evaluation of data in time and frequency domains, such as wavelet analysis, are employed [9]. These may be used to help identify the frequencies of interest and assist in development of subsequent less-expensive methods of detection.

This investigation is an extension of recent experimental work on cavitation in tip leakage flow using a single stationary hydrofoil analogy, where the effect of nuclei on cavitation in the flow were investigated [27, 26, 25]. Previous studies focused on two nuclei populations. The first population is characterized by a low concentration of nuclei with strong critical tension ever present in the water, and is labelled as 'natural nuclei population'. The second population is densely seeded with weak nuclei that can withstand very little tension and is labelled as 'abundant nuclei population'.

Current work adds data for an intermediate nuclei population consisting of weak nuclei, similar in strength to those characteristic of abundant nuclei populations, but in lower concentration (fig 2). This population is labelled as 'sparse nuclei population'. Along with a full acoustic and high-speed imaging dataset for sparse nuclei population, measurements are repeated for natural and abundant nuclei populations for a wider range of incidences. Acoustic spectra and wavelet analysis are used to investigate both incipient and developed cavitation, with an emphasis on the effect of nuclei on the incipient conditions, the flow topology and the acoustic signature.

2 Experiment Details

The experiments were performed in the University of Tasmania variable pressure water tunnel. The tunnel test-section is 0.6 × 0.6 m square at the entrance, by 2.6 m long. The operating velocity and pressure are controlled independently, with ranges from 2 to 13 m/s and 4 to 400 kPa absolute, respectively. The tunnel volume is 365 m^3 and is filled with demineralised water. Optical access is provided through acrylic windows on each side of the test-section. Further details on the facility are provided by [8, 7].

Tip gap flow was developed between the ceiling of the test-section and the end of a stationary hydrofoil, as schematically represented in figure 1. The hydrofoil model has a chord length of $c = 280$ mm. Section profiles for the model were designed using customised definitions for thickness and camber [28], and the geometry analysed using the 2D numerical code XFoil [15]. The tip section is analogous to a NACA 66-012 mod section with a NACA $a = 0.8$ rooftop camber profile, resulting in an overall flat pressure distribution with a maximum thickness of $t = 33.6$ mm. A cambered profile was used to increase lift, and care was taken during design to avoid cavitation on the face of the model. The section profile near the tip is held constant for a third of the hydrofoil span, but is thickened towards the base to reduce model vibration and any potential tip deflection under the load. A complex tip fairing was applied to avoid flow separation in the leakage flow. Further details on the model are provided in Russell et.al. [27].

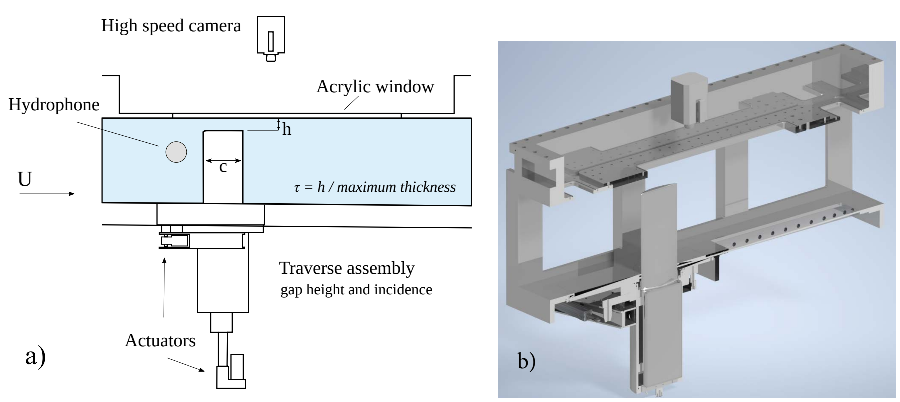

Fig. 1. a) Schematic of the experiment performed in the University of Tasmania cavitation tunnel. b) A 3D render of the experiment.

The hydrofoil was mounted in an actuated assembly that allowed for a continuous adjustment of the tip gap (h) and the incidence (α) of the hydrofoil. The actuators have an accuracy of 0.01 mm across a 300 mm travel, and for the present work the gap could be adjusted in the range $1 \leq h \leq 70$ mm. The range of incidence was $0° \leq \alpha \leq 10°$.

The hydrofoil tip gap was non-dimensionalised by the maximum thickness of the hydrofoil tip section, $\tau = h/t$, giving an approximate dimensionless clearance range of $0.03 \leq \tau = h/t \leq 2$. Reynolds number, based on a hydrofoil chord length of $c = 280$ mm, was held constant at $Re = Uc/\nu = 3 \times 10^6$, where U is the mean flow velocity and ν is the water kinematic viscosity. The cavitation number was defined as $\sigma = (p - p_v)/0.5\rho U^2$, where p is the static pressure at the tunnel ceiling, p_v is the water vapour pressure and ρ is the water density. The hydrofoil leading edge was located 900 mm downstream of the test-section entrance. At this position the unperturbed wall boundary layer thickness has been measured to be 19 mm [5].

The tunnel design enabled strict control of cavitation nuclei during the experiments. A dissolved oxygen concentration of approximately 30% of the value at atmospheric saturation was used to ensure the nuclei population remained stable. Alongside the natural nuclei population ever present within the tunnel, the experiments were performed for two seeded nuclei populations (sparse and abundant). The measured distributions of the three nuclei populations are presented in figure 2. Only one of these populations is activated at a time given their significant differences in susceptibility. If the artificially seeded population is used the natural population will remain inactive.

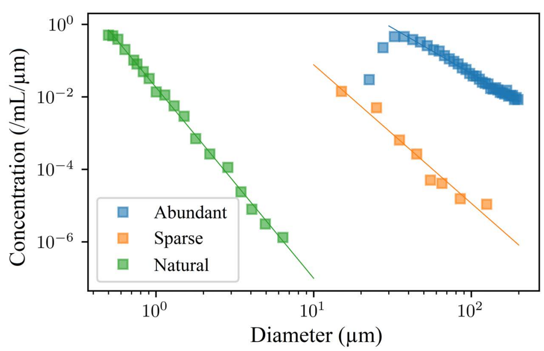

Fig. 2. Nuclei size distribution for the natural nuclei, and sparse and abundant polydisperse nuclei populations used in the experiments.

Acoustic measurements were obtained using a Brüel & Kjær Type 8103 hydrophone (voltage sensitivity 25.1 μV/Pa) mounted in a flooded cavity (kept at the same pressure as the tunnel test section) beneath a 10 mm polyurethane diaphragm with a 149 mm sensing diameter [13]. The hydrophone was mounted in the side wall, 150 mm below the test section ceiling and approximately a chord length upstream of the hydrofoil leading edge. The signal was conditioned using a Brüel & Kjær Nexus conditioner and amplifier, which was also used to apply a 0.1 Hz - 100 kHz bandpass filter. The filtered signal was acquired using a National Instruments PXIe-4497 card at a sampling rate of 204.8 kS/s. Each acoustic measurement was performed for a period of 60 s.

High-speed imaging of cavitation topology in the gap was acquired using a Phantom v2640 camera with a maximum resolution of 2048 × 1952 pixels, mounted above the tunnel test section. The camera was equipped with a Nikon AF Nikkor 24 mm f/2.8 D lens with the images acquired at a cropped resolution of 2048 × 640 pixels at a sampling rate of 10k frames per second. Continuous illumination was provided from two Effilux EFFI-BL-LITE-1M12P 650 × 650 mm LED panels mounted to the side of the test section and three Veritas Constellation 120 LED lamps mounted above and to the side of the test section. The image acquisition was controlled via Phantom PCC 3.4.4 software. Optical access to the gap was provided through a 1150 mm long × 215 mm wide acrylic window in the test section ceiling.

The high-speed imaging and the acoustic measurements were triggered independently, however, the data was synchronized by recording the camera trigger signal along with the acoustics and using it to align the two datasets. The camera was operated with a post trigger, so that once an incipient event was manually observed or heard, the camera trigger could be activated.

3 Spectral Analysis

Analysis of the acoustic data was performed using MATLAB software. An initial spectral survey was performed through Fourier analysis using the Welch estimate of the power spectral density [31]. Spectra obtained using this method would capture any large amplitude events or persistent changes at a given frequency across the 60 s duration of the data recording. This analysis successfully captured general trends within the data, and revealed marked differences in the acoustic signature for different nuclei populations and otherwise identical flow conditions. Sample results from these analyses are presented in figure 3 for cases with $\sigma = 3$ and $\sigma = 5$, for $\tau = 1$, and $\alpha = 5°$. For $\sigma = 5$ the flow is cavitation free providing a baseline case for comparison.

For the natural nuclei population and $\sigma = 3$, acoustic signature was characterised by a slight increase in PSD for frequencies around 300 Hz and above 10^4 Hz compared with the baseline. Nuclei contained in this population are small in size and require high tension for cavitation inception to occur. Although the flow generated sufficient pressure fluctuations to provide the tension required for these nuclei to be activated, the duration of incipient events at this 'near incipient' σ was short and the cavity quickly collapsed.

In similar investigations by Chang et. al. [10], they characterised such incipient events into two categories; 'chirps', and 'pops'. 'Pops' are extremely short in duration, < 2 ms, with the collapse of an incipient cavity accompanied with a broadband high frequency burst of sound. Meanwhile, 'chirps' are slightly longer in duration and more tonal in nature, producing noise at lower frequencies due to deformation of the cavity surface from oscillations in the surrounding vortex. Initiation of both types of cavitation are believed to occur due to unsteady stretching of small scale vorticity by larger structures [11, 2]. Due to their size, duration, and irregularity, these events were only captured in the acoustic data. It is suspected that they were either, occurring some distance downstream of the hydrofoil (outside the high speed camera field-of-view), or that these events are smaller than the resolvable scale of the used optical system.

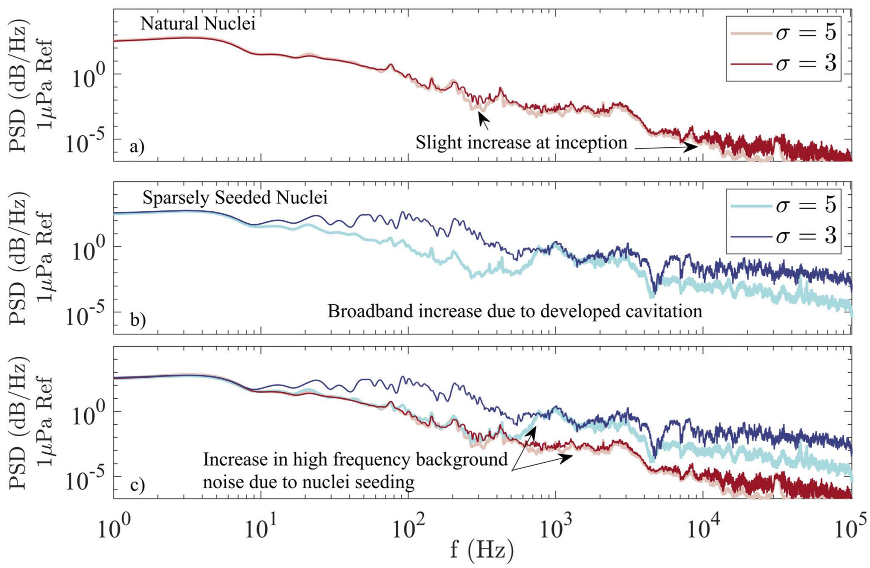

Fig. 3. (a-b) Spectra comparing acoustic measurements at $\sigma = 3$ to background acoustics at a higher cavitation number for $\alpha = 5^\circ$ and normalised gap height $\tau = 0.8$. Comparisons are made for a) the tunnel natural nuclei population, and b) with sparse nuclei seeding. c) Data from both nuclei populations are re-plotted on a common axis for direct comparison.

In contrast to the natural nuclei, addition of sparse nuclei for these flow conditions resulted in with well developed cavitation in the tip leakage vortex core. Nuclei in the seeded flow are one-to-two orders of magnitude larger than those characteristic of the natural nuclei population and, as such, have much lower critical tension. Consequently, where inception occurs only sporadically for the natural nuclei, an abundant influx of weak nuclei into the tip gap region in the seeded flow results in a persistent cavity filling the core of the tip-leakage vortex. The presence of a developed cavity imparted a broadband increase in the acoustic PSD across all frequencies above 10 Hz.

When the background acoustic data for natural and sparsely seeded nuclei populations are plotted together (fig 3c), an increase in PSD for the seeded flow is observed for the frequencies above 500 Hz. The observed increase in noise originates from the nuclei generators, and is associated with shear layer cavitation responsible for microbubble production [4].

Acoustic measurements were acquired for an extensive range of conditions. Data was captured for several tip gap clearances ranging between $0.1 \leq \tau \leq 1.8$, and an incidence range from $\alpha = 0°$ to $\alpha = 9°$ with a $1°$ increment. The measurements were obtained for three nuclei populations, and for multiple cavitation numbers ranging between $\sigma = 1$ and $\sigma = 5$. A representative sample of the spectra is presented for a cavitation number of $\sigma = 5$ in figure 4, and $\sigma = 3$ in figure 5. Amongst the wealth of information in these data some general trends are summarized below.

From an acoustic signature perspective the performance was worst for the flow sparsely seeded with nuclei. For this nuclei population an increase in noise levels was observed at lower incidences across the range of tested conditions. Further increase in microbubble concentration, i.e. for the abundant nuclei population, provided damping within the system, as the seeding bubbles started to accumulate within the core of the tip leakage vortex. The presence of non-condensable gas, not only dampens the shock-waves emitted during cavitation collapse [23], but also is likely to modulate the acoustic impedance within the flow surrounding the leakage vortex. In contrast, for the natural nuclei flow, this damping effect is not present, however, cavitation inception is delayed as the nuclei contained in the natural population are capable of withstanding significantly higher tension.

At low incidence ($\alpha \leq 3°$), a large peak in the acoustic spectra is noticeable for a frequency of 425 Hz. The amplitude of this peak is observed to decrease with increase in τ as α approaches $3°$. This trend persists across the range of cavitation numbers tested, which suggests that the source of this peak originates from the liquid phase.

Whilst the nature of this peak is currently unknown, there are two hypothesis for its origins. The first relates the peak to excitation of the standing acoustic modes within the tunnel. Estimates of standing acoustic mode frequency calculated using the tunnel dimensions match within an order of magnitude of the observed peak frequency. Supporting this idea is the absence of the peak in the spectra for the abundantly seeded flow, where a dense population of large bubbles may affect the sound speed and impedance within the flow.

The second hypothesis relates the spectral peak to the shedding at the trailing edge of the hydrofoil. The trailing edge thickness is about $h_{TE} = 2.2$ mm, which results in a trailing edge thickness-based Strouhal number $St = fh_{TE}/U_\infty = 0.107$. As discussed by Doolan et. al. [14], this agrees well with relations observed for trailing edge shedding about a NACA0012 hydrofoil section. Estimates of the bluntness parameter h_{TE}/δ^* support this hypothesis. In addition, RANS calculations of this geometry at $\alpha = 6°$ revealed a narrow region of flow separation near the trailing edge at the tip of the model [19]. However, due to an increase in the section thickness towards the root (due to structural considerations) the separated region becomes much larger. These hypotheses could be tested by altering the flow velocity within the tunnel, to determine whether there is a shift

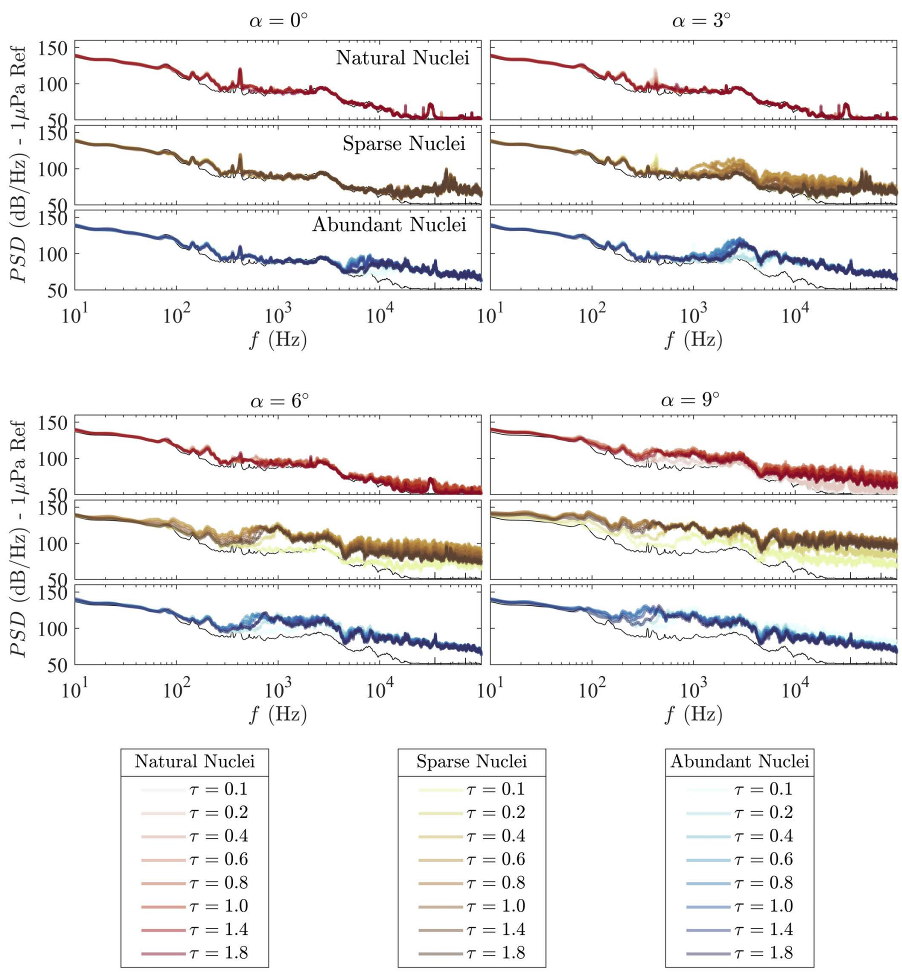

Fig. 4. Spectra recorded across a range of gap heights τ and incidence α for a cavitation number of $\sigma = 5$. For the majority of conditions only minimal cavitation is present, particularly for at low incidence. However for some conditions acoustic emissions from bubble excitation and incipient cavitation are present even at this high cavitation number. Generally, sparse nuclei populations and intermediate gap heights produce the most sound.

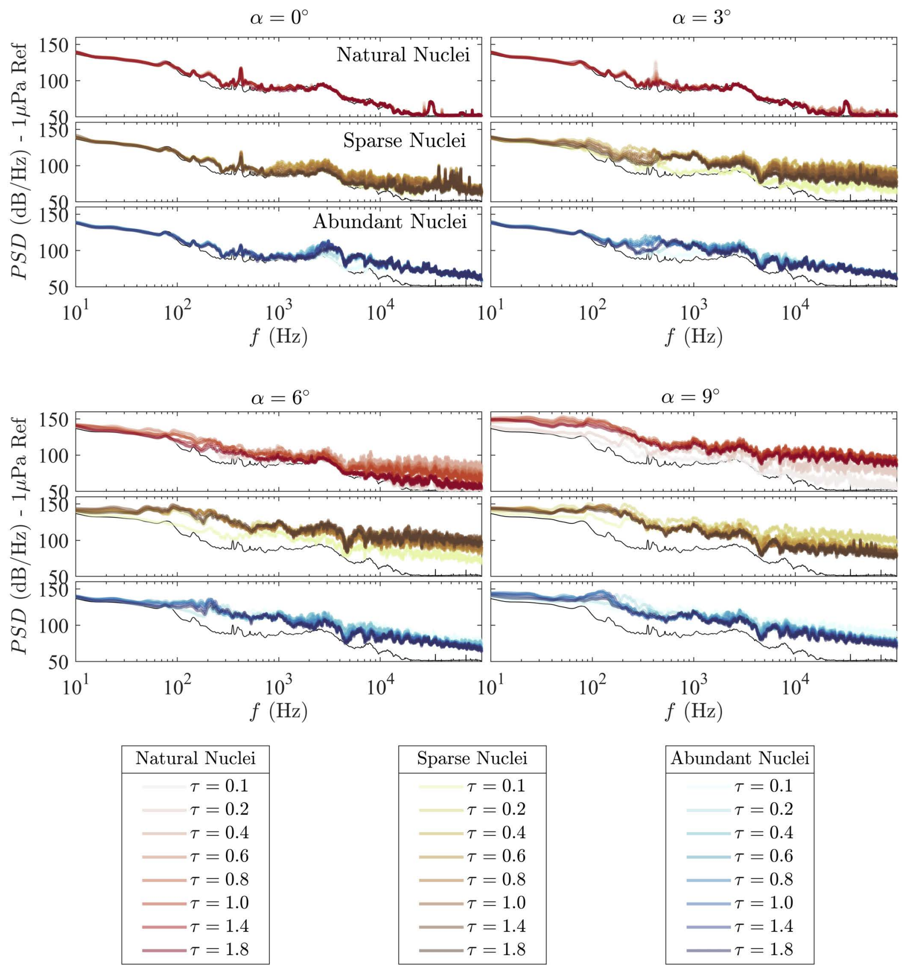

Fig. 5. Spectra recorded across a range of gap heights τ and incidence α for a cavitation number of $\sigma = 3$. For the majority of conditions plotted cavitation is well developed, particularly for condition which have been seeded with free-stream nuclei. Generally, sparse nuclei populations and intermediate gap heights produce the most sound.

in the peak frequency, or by placing an accelerometer on the model to confirm vibration. These test will be performed in the future.

Additional insights can be gained if the data are plotted as spectrograms with increasing incidence. These are plotted for each of the tested nuclei populations for a constant cavitation number of $\sigma = 3$ and a gap clearence of $\tau = 0.8$ (figure 6). The spectrograms are accompanied with sample images from the high-speed data that illustrate the extent of cavitation within the sparsely seeded flow with increasing incidence.

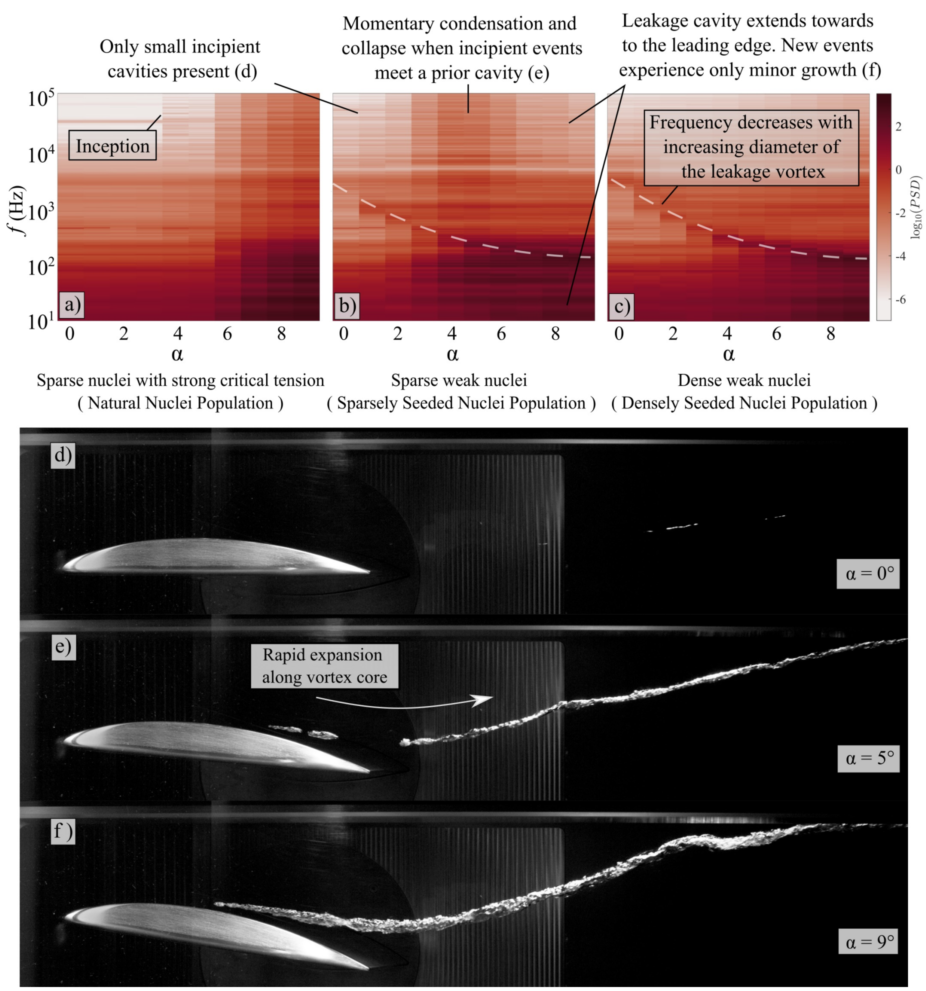

Fig. 6. (a-c) Spectrograms of the acoustic data for $\sigma = 3$, $\tau = 0.8$, for three nuclei populations within the test section. (d-f) Extracted frames from highspeed photography for the sparse seeded population, (b) in the spectrograms above.

For the natural nuclei, inception occurred at $\alpha \approx 4°$. Initially, the increase in spectral power is limited to mid-to-high frequencies; however, with incidence increasing past 6° a substantial increase in power is observed across all frequencies.

For the sparsely seeded flow cavitation is already present at $\alpha = 0°$, with an acoustic signature generally similar to that observed for incipient cavitation (at higher incidences) in the natural nuclei case. With an increase in α, the frequency of the tonal peak decreases (see dashed line in figure 6). A peak in high frequency power spectral density is observed for $\alpha \approx 5°$.

The origins of this peak have been discussed in Russell et. al. [27], where it was found that the rapid expansion of an emerging cavity and its coalescence with another cavity further downstream along the tip leakage vortex results in a pressure pulse. This process is illustrated in figure 6e. Merging of the two cavities often results in a localised and momentary cavity collapse, registered as an increase in the acoustic power spectral density.

At higher incidences the cavity fills the leakage vortex, with the cavity leading edge moving further upstream and closer to the low pressure face of the hydrofoil tip. Incipient cavities upstream of the cavity leading edge continue to occur, but grow to a smaller volume before coalescing with the pre-existing cavity. The smaller volume of these subsequent cavities results in a lower acoustic spike when merging with a pre-existing cavity.

A similar effect is seen in the abundantly seeded flow. Seeding bubbles accumulate within the core of the leakage vortex before inception has occurred. Due to the low critical tension and abundance of the seeding bubbles, tension within the core of the vortex cannot be sustained so there is no violent release upon inception. The same shift in tonal peak with increase in α is still observed as was seen in the flow with the sparse nuclei population.

From the high-speed imaging observations, the sliding tonal peak in the acoustic data can be correlated to the variation in the cavity volume and the rotation rate of the cavity surface (figure 7). The position of the tonal peak has been extracted from the spectra and is plotted across the range of investigated incidences and gap heights for a constant $\sigma = 3$. The trend observed in figure 6 persists for different gap heights, with the tonal peak frequency decreasing with an increase in α. While the form stays consistent as the angle of the hydrofoil is varied, a minimum in the tonal frequency is evident for an intermediate tip clearance $\tau \approx 0.8$.

When the gap is small, flow through the clearance is reduced. Cavity volumes are smaller leading to higher frequency oscillations. For large gap clearances, the trajectory of the leakage vortex remains close to the trailing edge and the leakage vortex rolls up cleanly in the wake of the hydrofoil [27]. For intermediate gap clearances, confinement leads to jetting of the tip gap flow and the leakage vortex is displaced further from the suction side of the hydrofoil. This results in a slight increase of the tip leakage vortex cavity diameter, which correlates with the decrease in the frequency of the spectral peak.

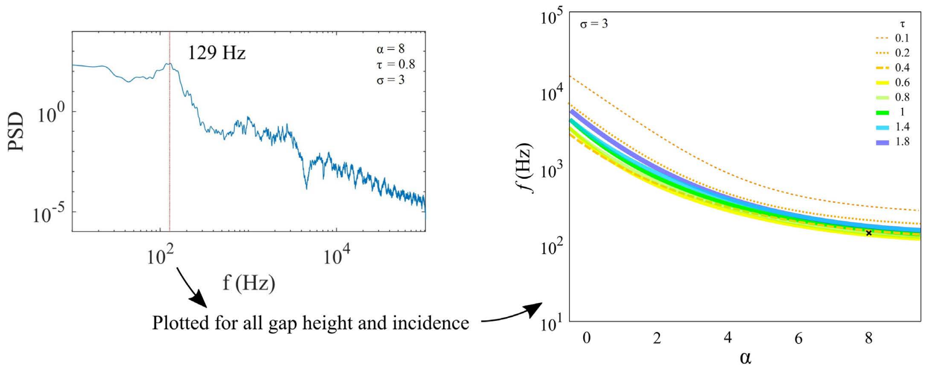

Fig. 7. The center of a broad peak is extracted from the acoustic spectra. Variation of the trend in peak frequency is plotted for gap height and incidence at $\sigma = 3$.

4 Cavitation intermittency in natural nuclei flow

For conditions near inception where both the amplitude of events and the event rate is low, spectral analysis may not be sensitive enough to provide meaningful information. This is particularly the case for the natural nuclei case, where the nuclei are very sparse.

To probe the data and ascertain the character of cavitation and inception, wavelet analysis using a MATLAB implementation of software by Torrence and Compo [30] was employed. Wavelet analysis has been proven to be an effective tool in the study of cavitation [9]. Inception in tip-leakage and shear flows is often characterized by short bursts of acoustic emissions that have been described as 'clicks' or 'pops' [11], for which wavelet analysis may be better suited than short-time Fourier analysis.

Normally, the continuous wavelet transform (CWT) is calculated from convolution of the acoustic data with scaled and translated versions of a mother wavelet Ψ_0. However, the method by Torrence and Compo [30] provides an efficient approximation to the CWT through application of the convolution theorem and the discrete Fourier transform of the hydrophone time series data. This allows the calculation of the wavelet to take place in Fourier space. Thus, for a given scale of the mother wavelet s, the transform for all $n = 1, 2, ..N$ points with spacing δt in the time-series are calculated simultaneously using

$$W_n(s) = \mathcal{F}^{-1}\left(\sum_{k=0}^{N-1} \hat{x_k}\hat{\Psi}^*(s\omega_k)e^{i\omega_k n\delta t}\right) \tag{1}$$

in which k denotes the index of the frequencies at which the discrete Fourier transforms are calculated.

A sixth degree Morlet wavelet was chosen as the 'Mother wavelet' as it provides a good compromise between time and frequency localisation. The complex wave function can extract both the amplitude and the phase at each scale, and is given by

$$\Psi_0(\eta) = \pi^{\frac{-1}{4}} e^{i\omega_0 \eta} e^{-\frac{1}{2}\eta^2} \tag{2}$$

where η is the non-dimensional time, and the non-dimensional frequency of oscillation in the mother wavelet $\omega_0 = 6$, the degree of the wavelet. To convert the frequency of the mother wavelet to a Fourier wavelength λ, multiplication by $(4\pi)/(\omega_0 + \sqrt{2+\omega_0^2})$ is required. Additionally in these calculations, a scaling is applied to Ψ from Ψ_0 to ensure the total energy of the wavelet at each scale is unity. A sample of the wavelet transform for a second of acoustic data is shown in figure 8. Here the PSD of the wavelet is calculated as $\|W_n(s)\|^2$.

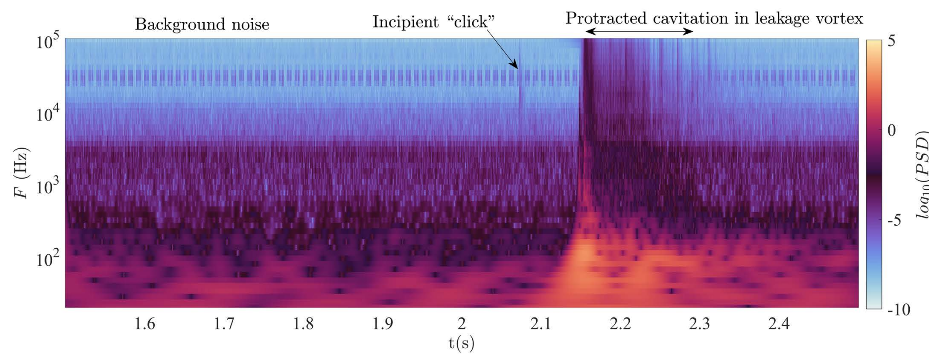

Fig. 8. Scaleogram of the wavelet transform for acoustic data at $\alpha = 6°$, non-dimensional gap height $\tau = 0.2$, and for a cavitation number of $\sigma = 2$ in which two incipient events are present.

From the wavelet analysis of the acoustic data for high σ values, where only a few events occur (such as depicted in figure 8), it can be seen that incipient events result in a broadband increase in power relative to the background noise. With increase in cavitation extent, the affected frequency range expands from a very high frequency band in the range 10 kHz$\leq f \leq$ 100 kHz for the small incipient structures, to frequencies as low as 100 Hz for more developed cavities. Nevertheless, all incipient events impart some increase in power for frequencies above 50 kHz.

From this observation a less computationally expensive method for the detection of incipient events in the flow populated with natural nuclei was developed. In addition, this feature was also used to determine the proportion of time for which cavitation was present. The method is adapted from processing techniques used for the detection of nuclei activations in a cavitation susceptibility meter and is divided into five stages [22].

1. High-pass filtering (cut-off frequency $f_c = 50$ kHz)
2. Rectification (To make all fluctuations of the same sign)
3. Low-pass filtering (To smooth fluctuations into a single event)
4. Log-scaling (To amplify small peaks)
5. Thresholding (To determine when an event has occurred)

An example of these processes being applied to raw data is presented in figure 9. The final step of the analysis was to calculate the fraction of the time that acoustic pressure exceeds a threshold value indicative of cavitation. The contours in figure 10 delineate these regions as a percentage.

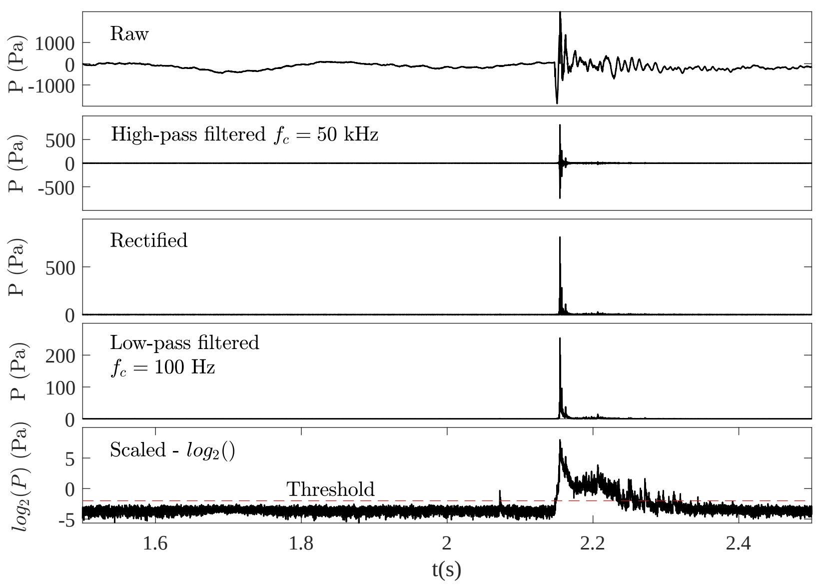

Fig. 9. Process of cavitation inception detection from acoustic data in the deplete population. A larger cavity is preceded by a smaller incipient event. (See figure 8 for the wavelet transform). Recorded for $\alpha = 6°$, non-dimensional gap height $\tau = 0.2$, and for a cavitation number of $\sigma = 2$. The threshold for cavitation detection was set at $log_2(P) = -2$ Pa.

Even for the natural nuclei flow, where tension required for nuclei activation was high, cavitation for the hydrofoil at a high incidence could not be suppressed for all but the lowest gap clearances. By stipulating that inception occurs when the acoustic signal is above the selected threshold for at least 2% of time, inception for $\tau = 0.8$ and $\sigma = 4$ occurred for $\alpha = 7°$. With an increase in gap clearance the incipient incidence increased to $\alpha = 8°$, while by reducing the gap towards the minimum value of $\tau = 0.1$ inception was delayed until $\alpha = 10°$. These findings are consistent with the previous study [27], where the incipient event rate was higher for intermediate gap heights near $\tau = 1$. As expected, a decrease in the cavitation number leads to inception at a lower incidence. The peak in cavitation activity at intermediate gap heights still remained, but becomes less prominent with decrease in σ.

5 Discussion

The persistence and nature of cavitation in the leakage vortex is sustained by three main influences. The event rate of new cavities, the duration for which a cavity can be sustained, and the speed at which an established cavity is advected downstream. Together these features control the spread between inception and constant cavitation as shown in figure 10.

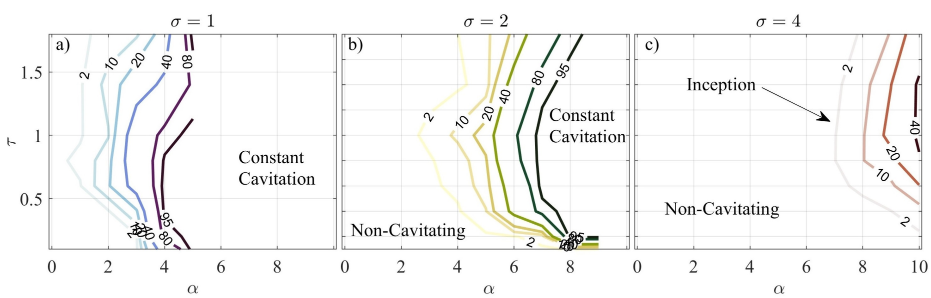

Fig. 10. Intermittency of cavitation within acoustic data is presented as a proportion (%) of the signal for which cavitation was detected. (a-c) Contours for three cavitation numbers map changes with gap height and incidence.

Further insights into the peak in the cavitation activity for an intermediate gap clearance can be gained from high-speed imaging. For low σ values, incipient cavities grow in both directions along the axis of the tip leakage vortex core. However, due to local advection of the vortex core, cavities are slowly advected downstream until they are eventually washed away.
At small gap heights where the tip flow remains affected by the wall boundary layer, low momentum fluid is ingested into the vortex core, and as a result downstream advection of the cavities is slower relative to the free-stream flow. Conversely at large gap clearances, flow rolls-up into the leakage vortex so that the velocity at the core exceeds the freestream flow.
Measurements of the vortex strength have been reported by Dreyer et. al [16] using particle image velocimetry, including the measurements of variation of streamwise velocity. They describe the phenomena related to variation in streamwise velocity with the gap clearance as a balance between a 'wake-like' and 'jet-like' streamwise velocity profile. Therefore, for different τ values it will take a varying amount of time before the leakage flow is free of cavitation following an incipient event. In addition to these processes, the availability of freestream

nuclei alters the inception rate of new cavities. If the incipient event rate is faster than the time it takes for the cavity to be washed away, cavitation will persist constantly within the leakage vortex.
Things are slightly more complex at higher cavitation numbers. In near inception conditions the cavity may collapse before it is washed away as the pressure recovers along the core of the leakage vortex. This is also true for low τ values, where the leakage vortex is less coherent and the instantaneous pressure fluctuations that characterize inception for these conditions are short lived. As discussed previously, it is in-between these two extremes where the loudest acoustic signature is produced.

6 Conclusions

The nature of cavitation associated with tip leakage flow for a range of influences are assessed. Measurements include variation of the cavitation number, tip gap clearance, incidence, and nuclei population. Incipient event rates are controlled by the spatio-temporal concurrence of captured nuclei and low pressures that occur within vortical structures of tip leakage flow. The former is controlled principally by the nuclei population and the nature of the turbulent flow, whereas the latter is largely influenced by the cavitation number and the strength of the primary vortex. The vortex in turn is determined by the combined effect of the tip gap and the hydrofoil incidence. It is the combined effect of the incidence and tip gap clearance that control not only the strength of the primary vortex, but also the axial velocity within the core of the vortex. This controls the period of incipient events, their residence in the vortical structures and whether they occur in isolation or interact. The strength and concentration of the nuclei population determine whether cavitation occurs as isolated violent events or a high void fraction bubble flow. These conditions lead to diverse acoustic signatures that require equally diverse analysis techniques to capture their respective features.

Acknowledgments

This project was supported by the US Office of Naval Research and ONR Global through NICOP S&T Grant no. N62909-19-1-2062, and the 2019 U.S. Multidisciplinary University Research Initiative (MURI) and the Australian Defence Science and Technology Group (DSTG). The authors are grateful for the technical assistance provided by Mr. Steven Kent and Mr. Robert Wrigley when conducting these experiments.

References

1. Agarwal, K., Ram, O., Lu, Y., Katz, J.: On the pressure field, nuclei dynamics and their relation to cavitation inception in a turbulent shear layer. Journal of Fluid Mechanics **966**, A31 (2023). https://doi.org/10.1017/jfm.2023.368

2. Allan, E.S.C., Barbaca, L., Venning, J., Russell, P., Pearce, B., Brandner, P.: Nucleation and Cavitation Inception in High Reynolds Number Shear Layers. Physics of Fluids **35**(1), 013317 (2023). https://doi.org/10.1063/5.0132054
3. Arndt, R.E.: Cavitation in vortical flows. Annual Review of Fluid Mechanics **34**(1), 143–175 (2002). https://doi.org/10.1146/annurev.fluid.34.082301.114957
4. Barbaca, L., Russell, P.S., Pearce, B.W., Brandner, P.A.: Characterization of microbubble generation in a confined turbulent jet. p. Paper. The University of Queensland, Brisbane, Australia (Dec 2020). https://doi.org/10.14264/36f5f4c
5. Belle, A., Brandner, P., Pearce, B., de Graaf, K., Clarke, D.: Artificial Thickening and Thinning of Cavitation Tunnel Boundary Layers. Experimental Thermal and Fluid Science **78**, 75–89 (2016). https://doi.org/10.1016/j.expthermflusci.2016.05.007, req:
6. Brandao, F.L., Mahesh, K.: Large–eddy simulation of cavitation inception in a shear flow. International Journal of Multiphase Flow **146**, 103865 (2021). https://doi.org/10.1016/j.ijmultiphaseflow.2021.103865
7. Brandner, P., Lecoffre, Y., Walker, G.: Development of an Australian National Facility for cavitation research. MARIN, Wageningen, The Netherlands (Sep 2006)
8. Brandner, P., Lecoffre, Y., Walker, G.: Design considerations in the development of a modern cavitation tunnel. In: 16th Australasian Fluid Mechanics Conference. Gold Coast, Australia (2007)
9. Brandner, P.A., Venning, J.A., Pearce, B.W.: Wavelet analysis techniques in cavitating flows. Philosophical transactions of the Royal Society of London. Series A: Mathematical, physical, and engineering sciences **376**(2126) (2018). https://doi.org/10.1098/rsta.2017.0242, req:
10. Chang, N.A., Ceccio, S.L.: The acoustic emissions of cavitation bubbles in stretched vortices. Journal of the Acoustical Society of America **130**(5), 3209–3219 (2011). https://doi.org/10.1121/1.3626121, http://pdfserv.aip.org/JASMAN/vol_130/iss_5/3209_1.pdf
11. Chesnakas, C.J., Jessup, S.D.: Tip-vortex induced cavitation on a ducted propulsor. Honolulu, Hawai, USA (Jul 2003). https://doi.org/10.1115/FEDSM2003-45320, available from ASME digital store
12. Choi, J., Chang, N., Yakushiji, R., Dowling, D.R., Ceccio, S.L.: Dynamics and noise emission of vortex cavitation bubbles in single and multiple vortex flow. MARIN, Wageningen, The Netherlands (Sep 2006)
13. Doolan, C., Brandner, P., Butler, D., Pearce, B., Moreau, D., Brooks, L.: Hydroacoustic characterisation of the AMC cavitation tunnel. The Australian Acoustical Society, Victor Harbor, Australia (Nov 2013)
14. Doolan, C., Moreau, D.: Flow Noise: Theory. Springer Singapore, 1 edn. (2022). https://doi.org/https://doi.org/10.1007/978-981-19-2484-2
15. Drela, M.: XFOIL: An analysis and design system for low Reynolds number airfoils. Lecture Notes in Engineering, vol. 54, pp. 1–13. Springer-Verlag, Notre dame, Indiana, USA (Jun 1989)
16. Dreyer, M., Decaix, J., Münch-Alligné, C., Farhat, M.: Mind the gap: a new insight into the tip leakage vortex using stereo-PIV. Experiments in Fluids **55**, 1849 (2014). https://doi.org/10.1007/s00348-014-1849-7
17. Gopalan, S., Katz, J., Liu, H.L.: Effect of gap size on tip leakage cavitation inception, associated noise and flow structure. Journal of Fluids Engineering **124**(4), 994–1004 (Dec 2002). https://doi.org/10.1115/1.1514496
18. Gopalan, S., Liu, H.L., Katz, J.: On the flow structure, tip leakage cavitation inception and associated noise. pp. 639–653. Val de Reuil, France (Sep 2000), http://www.me.jhu.edu/ lefd/jet/23NavalHydro.pdf

19. Jin, Y., Pook, D., Venning, J.A., Barbaca, L., Russell, P.S., Pearce, B.W., Brandner, P.A.: Computational study of tip leakage flow around a static hydrofoil. In: 23rd Australasian Fluid Mechanics Conference. The University of Sydney, The University of Sydney (2022). https://doi.org/http://www.afms.org.au/proceedings/23.html
20. Judge, C.Q., Oweis, G.F., Ceccio, S.L., Jessup, S.D., Chesnakas, C.J., Fry, D.J.: Tip-leakage vortex inception on a ducted rotor. In: Fourth International Symposium on Cavitation. California Institute of Technology (2001). https://doi.org/http://resolver.caltech.edu/CAV2001:sessionA6.001
21. Khoo, M.T., Venning, J.A., Pearce, B.W., Brandner, P.A.: Nucleation and cavitation number effects on tip vortex cavitation dynamics and noise. Experiments in Fluids **62**, 216 (2021). https://doi.org/10.1007/s00348-021-03308-2
22. Khoo, M.T., Venning, J.A., Pearce, B.W., Brandner, P.A., Lecoffre, Y.: Development of a cavitation susceptibility meter for nuclei size distribution measurements. In: 20th Australasian Fluid Mechanics Conference. AFMS, Perth, Australia (2016)
23. Mäkiharju, S.A., Ganesh, H., Ceccio, S.L.: The dynamics of partial cavity formation, shedding and the influence of dissolved and injected non-condensable gas. Journal of Fluid Mechanics **829**, 420–458 (2017)
24. Oweis, G.F., Fry, D., Chesnakas, C.J., Jessup, S.D., Ceccio, S.L.: Development of a tip-leakage flow — Part 1: The flow over a range of Reynolds numbers. Journal of Fluids Engineering **128**(4), 751–764 (Jul 2006). https://doi.org/10.1115/1.2201616
25. Russell, P.S., Barbaca, L., Russell, E.S.C., Pearce, B.W., Brandner, P.A.: Cavitation in tip-leakage flows. In: 33rd Symposium on Naval Hydrodynamics. Osaka, Japan (2020)
26. Russell, P.S., Barbaca, L., Venning, J.A., Pearce, B.W., Brandner, P.A.: Nucleation effects on tip-gap cavitation. In: 22nd Australasian Fluid Mechanics Conference. The University of Queensland, Brisbane, Australia (2020). https://doi.org/https://doi.org/10.14264/da5bd86
27. Russell, P.S., Barbaca, L., Venning, J.A., Pearce, B.W., Brandner, P.A.: The influence of nucleation on cavitation inception in tip-leakage flows. Physics of Fluids **35**(1) (2023). https://doi.org/10.1063/5.0132034
28. Russell, P., Pearce, B., Brandner, P.: A method for generating lifting surface profiles from simplified parametric equations. In: 23rd Australasian Fluid Mechanics Conference. The University of Sydney, Sydney, Australia (2022). https://doi.org/http://www.afms.org.au/proceedings/23.html
29. Temperley, H., Chambers, L.: The behaviour of water under hydrostatic tension: I. Proceedings of the Physical Society **58**(4), 420–436 (1946). https://doi.org/10.1088/0959-5309/58/4/310
30. Torrence, C., Compo, G.P.: A practical guide to wavelet analysis. Bulletin of the American Meteorological Society **79**(1), 61–78 (1998). https://doi.org/10.1175/1520-0477(1998)079<0061:APGTWA>2.0.CO;2
31. Welch, P.D.: The use of fast fourier transform for the estimation of power spectra: A method based on time averaging over short, modified periodograms. IEEE transactions on Audio and Electroacoustics **15**(2), 70–73 (1967). https://doi.org/http://dx.doi.org/10.1109/TAU.1967.1161901